Life-Cycle of Structures and Infrastructure Systems – Biondini & Frangopol (Eds)

Durability analysis and optimization of a prestressed concrete bridge strengthened by a fiber reinforced concrete layer

S. Schoen, P. Edler & G. Meschke
Institute for Structural Mechanics, Ruhr University Bochum, Germany

S. Freitag
Institute for Structural Analysis, Karlsruhe Institute of Technology, Germany

ABSTRACT: The durability of reinforced concrete (RC) structures is influenced by uncertain service loads and material properties, which must be taken into account in service life-oriented structural design. The consideration of aleatory and epistemic uncertainties allows probabilistic service life predictions in the context of service life design, replacing the classical safety factors.

In the context of this article, the service life of a prestressed concrete bridge strengthened with a fiber reinforced concrete (FRC) layer is to be maximized. The L3378 bridge near Fulda-Lehnerz in Germany will be used as a reference structure. The bridge consists of four prefabricated prestressed RC girders with T-girder cross-section, supplemented by an RC layer and an additional FRC layer. The FRC layer is made of ultra-high-performance fiber reinforced concrete (UHPFRC) and is intended to increase the load-bearing capacity while also serving as a waterproofing layer.

For the optimization, finite element simulations are performed to determine the most sensitive parameters. The fiber orientation of the UHPFRC layer, the prestressing force and position, the bond between concrete and steel, and the material properties are investigated, and then the most sensitive parameters are applied as uncertain parameters for the maximization of the service life, while the cost of material is to be minimized. Although the reference structure is build new, the presented design approach is also applicable to the strengthening of existing structures to extend their service life. For this reason, the original design is finally compared with a conventional design without FRC layer in terms of failure probability considering stochastic live loads and polymorphic uncertainties.

1 INTRODUCTION

Reinforced and prestressed concrete bridges are designed for a long service life, but often have to be repaired at an early stage due to excessive cracks. One way to minimize these cracks, is the use of alternative materials such as fiber-reinforced concrete (FRC). FRC combines conventional concrete with randomly oriented fibers added during the mixing process. These fibers improve the concrete ductility after cracking, which is traditionally remedied with reinforcement. FRC can be specifically customized to meet particular requirements due to different fiber materials including steel, glass and carbon fibers, different fiber geometries such as microfibers or macrofibers with different anchorage, different fiber content, and a variety of concrete mixture (Holschemacher et al. 2017). One example is the bridge L3378 near Fulda-Lehnerz in Germany, which is strengthened by an additional thin ultra-high-performance fiber reinforced concrete (UHPFRC) layer, while the rest of the cross-section consists of reinforced normal weight concrete (RC). This UHPFRC layer consists of an ultra-high strength concrete with steel micro fibers (Pelke et al. 2018). Difficulties arise in the design of bridges with FRC, because there are currently no adequate design codes for the design of FRC structures. For this reason, within the scope of this paper, a reliability design optimization approach considering polymorphic uncertainties (Edler et al. 2019) is applied to reduce the required steel reinforcement. Aleatory uncertainties are characterized by a known variability given by a large number of data, and therefore, are modeled by stochastic

DOI: 10.1201/9781003323020-57

distributions. However, if only a few data is available, i.e. a lack of knowledge (e.g. the fiber orientation), it is called epistemic uncertainty and modeled by intervals or fuzzy numbers (Möller & Beer 2008). In the context of this paper, aleatory and epistemic uncertainties are intended to replace classical safety factors. For the optimization, a multilevel model is utilized for the analysis of FRC structures, whereby the influence on the structural response can be directly evaluated based on a selected fiber type, content and orientation (Zhan & Meschke 2016). The post-cracking behavior of plain concrete (PC), RC, and FRC structures using finite element (FE) analysis is described by a discrete crack approach using interface elements (Ortiz & Pandolfi 1999). The post-cracking behavior is derived from the tensile separation law for the particular material.

2 MATERIAL MODEL FOR REINFORCED CONCRETE AND FIBER REINFORCED CONCRETE

A discrete crack finite element model (Ortiz & Pandolfi 1999) is utilized to model the cracking behavior of concrete under tension. This model is characterized by cohesive interface elements, which are inserted between linear-elastic triangular finite elements (i.e. bulk elements). The fracture behavior of plain and fiber reinforced concrete is modeled by the sum of two separate nonlinear traction-separation laws $\boldsymbol{t} = \boldsymbol{t}^{\text{concrete}} + \boldsymbol{t}^{\text{fibers}}$ within the integration point of each of the interface element.

2.1 *Material model for plain concrete*

Considering the behavior of plain concrete with exponential softening first, we obtain the following traction-separation relationship

$$t^{\text{concrete}}(\omega) = f_{ct} \exp\left(-\frac{\omega f_{ct}}{G_f}\right), \tag{1}$$

where ω is the effective crack separation (Gudzulic & Meschke 2021), f_{ct} the tensile strength and G_f the fracture energy.

2.2 *Extension for fiber reinforced concrete*

Once cracks initiate in FRC, fibers provide a bridging traction acting on the crack faces to keep the crack width small. This is considered via the traction-separation relationship $t^{\text{fibers}}(\omega)$, which takes also the fiber orientation and the fiber geometry into account. This traction-separation relationship is determined by integrating the pullout force-displacement relations $F(\omega, \theta, \tilde{x})$ of all crack-bridging fibers, taking into account their inclination to the crack surface θ and the embedding lengths $\tilde{x}$. This results, according to Wang et al. (1989), in a function of the smeared fiber pull-out forces

$$t^{\text{fibers}}(\omega) = \frac{c_f}{A_f} \cdot \int_0^{L_f/2} \left[\int_0^{\text{acos}\left(2\tilde{x}/L_f\right)} F(\omega, \theta, \tilde{x}) p(\theta) \mathrm{d}\theta \right] p(\tilde{x}) \mathrm{d}\tilde{x}, (2) \tag{2}$$

where c_f describes the volume fraction A_f and L_f the fiber cross section and the fiber length, respectively, and $p(\theta)$ the probability density of the fiber orientation. The spatial orientation of the fibers depends on the dimensions of the structural component and the casting direction. In order to take these factors into account, a method to calculate the probability density $p(\theta)$, based on a given fiber orientation profile $\lambda_{cast} = [a, b, c]$ was developed in Zhan & Meschke (2016). Here, an ellipsoid represents the spatial preference of fibers in the global coordinate system (Figure 1, center). It should be noted that an isotropic fiber orientation is described graphically by a sphere with the fiber orientation profile $\lambda_{cast} = [0.33, 0.33, 0.33]$. Considering a homogeneous fiber distribution, within the structural component, $p(\tilde{x})$ is equal to $\frac{L_f}{2}$ (Wang et al. 1989). Since obtaining the traction-separation relationship of the fiber-reinforced

concrete can only be evaluated numerically, it is replaced within the FE model by an analytical, parameterized surrogate function

$$t^{\text{fibers}}(\omega) = t_1\left(\omega_u - \frac{\omega}{\omega_u}\right) + t_2\omega\exp(c_1 - c_2\omega). \tag{3}$$

The coefficients t_1, t_2, c_1, c_2 are determined by fitting the surrogate function to the numerical evaluation of Eq. 2 and w_u represents the ultimate crack opening.

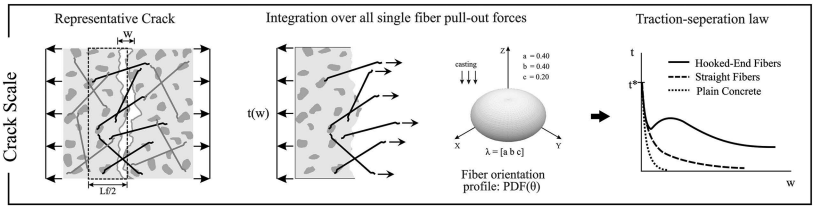

Figure 1. Multi-level modelling of FRC. Integration of the pull-out response of all fibers crossing a representative crack and considering their orientation to calculate the traction-separation law.

2.3 *Embedded rebar model*

The reinforcement is considered by a discretization-independent embedded rebar model with geometrically linear truss elements. The properties of steel are taken into account with an elastoplastic material behavior using the v. Mises yield criterion with linear hardening. The interaction between reinforcing steel and concrete is considered with a bond-slip law using the *fib* Model Code 1990. The internal force contribution of the reinforcement slip with respect to the bulk matrix is penalized to enforce a displacement constraint between the rebar and the concrete (Gall et al. 2018).

3 BRIDGE WITH ULTRA-HIGH-PERFORMANCE CONCRETE LAYER

The bridge L3378 has a standard RQ 11 cross-section with two lanes and a width of 8.0 m. The structure replaces a two-span, flat-founded reinforced concrete slab girder from 1967, whose condition rating had dropped to 3.5 in the last structural inspections. A repair was not economical due to the continued increase in traffic load. The new design includes the two-span prestressed concrete deck with span widths of 17.10 m and 20.41 m and a total static height of 1.05 m. The cross-section contains three different horizontal components. The base consists of 2 single-span girders, each consisting of four T-shaped precast prestressed concrete girders of strength class C45/55 with a height of 0.85m (see Figure 2a). The precast concrete is supplemented by a 0.13m thick in-situ concrete of strength class C35/45. The cross-section is finished horizontally at the top with a 0.07m thick reinforced ultra-high-performance reinforced concrete (UHPRC) layer strengthened with steel microfibers (Pelke et al. 2018). The final bridge is presented in Figure 2b and the material properties are listed in Tables 1 and 2.

3.1 *Sensitivity analysis*

Since usually a large number of realizations is needed for probabilistic service life prediction, the bridge is reduced to a 2D model with a constant line load of q = 100 kN/m. The microfibers in the top layer are used to limit the cracks at the middle support, but this is only possible if the fibers are aligned longitudinally to the beam. The fiber orientation is considered by a spherical distribution of the probability density function $p(\theta)$ (see Eq. 2), with the orientation profile $\lambda_{cast} = \left[\lambda_f, \frac{1-\lambda_f}{2}, \frac{1-\lambda_f}{2}\right]$. The semi-major axis λ_f is modeled as an interval $\lambda_f = [0.30, 0.45]$. This interval bandwidth is based on the experimental results of Tiberti et al. (2018), where 140 equally sized bending beams with two different casting processes were examined with respect to their fiber orientation within the cross section. The measured inclination between 53.1° and 34.9° corresponds to the fiber orientation parameter λ_f in the range of 0.30 to 0.45.

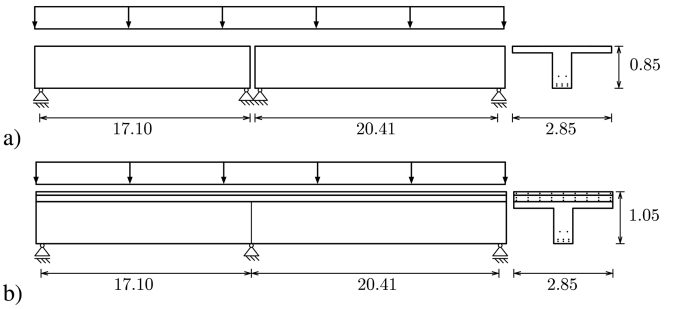

Figure 2. Schematic representation of the bridge a) in the first state of construction and b) in the final state of construction.

Table 1. Material properties of concrete.

Property		C45/55	C35/45	UHPC	HPC	Unit
Young's modulus	E	36,000	34,000	50,000	40,000	[N/mm^2]
Poisson's ratio	ν	0.2	0.2	0.2	0.2	[-]
Tensile strength	f_{ct}	3.8	3.2	11	7	[N/mm^2]
Compressive strength	f_{cm}	53	43	167.5	80	[N/mm^2]
Fracture energy	G_f	0.148	0.143	0.181	0.15	[N/mm]
Volume fraction	c_f	-	-	150	60	[kg/m^2]

Table 2. Material properties of steel.

Property		St1570/1770	B500	Unit
Young's modulus	E	195,000	200,000	[N/mm^2]
Yield stress	σ_{ys}	1770	500	[N/mm^2]

In Figure 3a), the maximum crack width w_{max} at the top edge of the cross-section is plotted as a function of the applied load q for different cases of fiber orientation within the UHPRC layer. Contrary to expectations, the fiber orientation has an influence on the initiation of the cracks at the top edge. This is due to the fact that the in-situ concrete layer has a significantly lower tensile strength than the fiber-reinforced concrete layer, and thus, the in-situ concrete layer starts to crack first (see Figure 4b)). Consequently, the crack starts in the middle of the cross-section and grows towards the top. Especially with horizontal fiber orientation ($\lambda_f = 0.45$), this crack propagation is limited through the fibers. However, as soon as the crack reaches the upper edge, the fibers can hardly limit the crack width, since even with horizontal fiber orientation ($\lambda_f = 0.45$), the crack width increases rapidly. Nevertheless, the maximum allowable crack width of $w_{crit} = 0.2$ mm according to Eurocode 2 is maintained for all three cases at the design load of q = 100 kN/m.

Beside the fiber orientation, the crack width may be influenced by other effects, e.g. an increase in the design load or a decrease in the prestressing force. Both scenarios are likely to happen in reality. For example, due to creep and shrinkage of the concrete, the prestressing force is time-variant, i.e., not equal to the initially applied prestressing force. This loss depends on various factors such as the age of the concrete, temperature and humidity during prestressing. For simplicity, according to the design guidelines (Eurocode 2) for this structure, a prestressing loss of 15% may be considered. To illustrate the influence of the prestressing loss, the maximum crack width w_{max} is plotted as a function of the applied load q for $\lambda_f = 0.45$ and $P_{\text{loss}} = 15\,\%$ in Figure 3 a), as well. Here, even for a horizontal fiber orientation ($\lambda_f = 0.45$) at the design load of q = 100 kN/m the maximum crack width $w_{cr} = 0.27$ mm is clearly above the maximum allowable crack width of $w_{crit} = 0.2$ mm (Eurocode 2).

In the following, an alternative design (variant B) will be investigated. In order to better emphasize the positive effects of fiber-reinforced concrete, the upper two layers are combined,

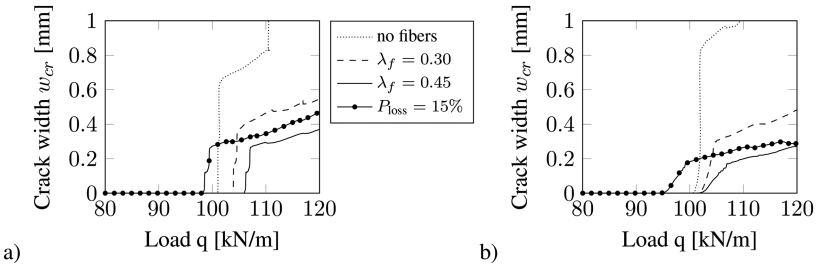

Figure 3. Crack width depending on the load for different fiber orientation and different prestressing force for a) variant A and b) variant B.

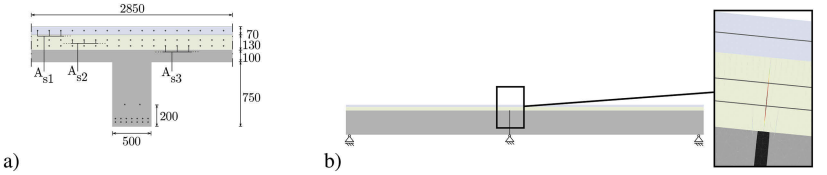

Figure 4. Illustration of crack initiation of variant A.

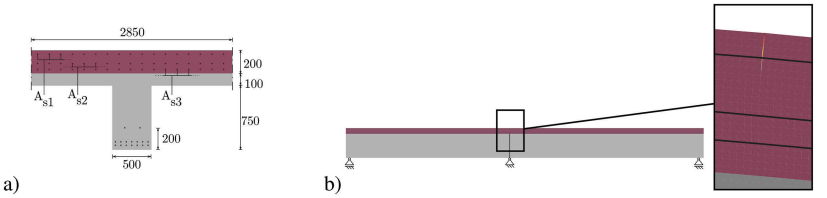

Figure 5. Illustration of crack initiation of variant B.

meaning the bridge consists of the prestressed precast beam and a 0.2 m thick fiber-reinforced HPC layer (see Figure 5a). The material properties are summarized in Table 1. Since fibers with hook end are able to limit the crack width even better than normal fibers or microfibers, for variant B steel fibers of type DRAMIX 60 are utilized. The use of such steel fibers in HPC has already been validated in Gudzulic et al. (2020). In Figure 3b), the maximum crack width w_{max} is plotted as a function of the applied load q for the same scenarios as for the original design (variant A). In variant B due to the significantly lower tensile strength compared to variant A, cracking begins at a lower applied load q. However, especially in case of fibers with horizontal orientation ($\lambda_f = 0.45$), the crack width is limited even at a higher loads. Moreover, with horizontal fiber orientation ($\lambda_f = 0.45$) and a prestressing loss of $P_{\text{loss}} = 15\,\%$, the maximum crack width ($w_{cr} = 0.18$ mm) is beneath the maximum allowable crack width of $w_{crit} = 0.2$ mm at the design load of q =100 kN/m.

3.2 *Reliability design optimization*

In the following, a reliability design optimization is performed for variant A and variant B considering uncertainties in loading, prestressing loss and fiber orientation. In addition, a reliability design optimization for a third variant (variant B0), which investigates the influence of fibers on the objective function, is performed. For this purpose, variant B was modeled without fibers. In other words, for variant B0 all material properties and layer thicknesses correspond to those of variant B and only the top layer is high performance concrete (HPC), instead of a high performance fiber reinforced concrete (HPFRC). Due to more steel fibers in variant B compared to variant A and variant B0, the aim is to reduce the steel reinforcement, to save costs, by still maintaining the serviceability. The objective is to minimize the total steel reinforcement A_s at the

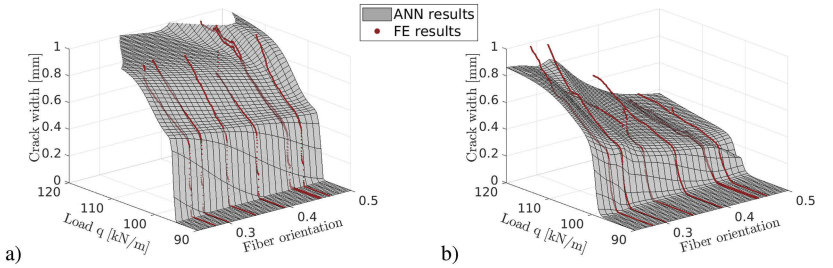

Figure 6. Crack width depends on the load and the fiber orientation for a fixed prestressing loss of $P_{\text{loss}} = 10\,\%$ and amount of reinforcement of $A_{s1} = 18\varnothing 16\text{mm}$, $A_{s2} = 14\varnothing 14\text{mm}$ and $A_{s3} = 0$ for a) variant A and b) variant B.

middle support by constraining the failure probability, which is based on a maximal acceptable crack width of $w_{cr} = 0.2\text{mm}$. This can be formulated for variant A and B as

$$\begin{aligned} &\min: \quad \hat{Z}(A_s) = A_s \\ &\text{s.t.}: \quad c(A_s, q, \lambda_s, P_{\text{loss}}) = P_f\left(\omega_{cr}\left(A_s, q, \lambda_f, P_{loss}\right) \leq 0.2\right) - P_{f,acc} \leq 0, \end{aligned} \tag{4}$$

and for variant B0 as

$$\begin{aligned} &\min: \quad \hat{Z}(A_s) = A_s \\ &\text{s.t.}: \quad c(A_s, q, P_{\text{loss}}) = P_f(\omega_{cr}(A_s, q, P_{loss}) \leq 0.2) - P_{f,acc} \leq 0. \end{aligned} \tag{5}$$

In Eq.4 and 5, the accepted probability of failure is described by $P_{f,acc} = \Phi(-\beta)$, where Φ is the cumulative distribution function of the standard normal distribution and β is the reliability index, which is set to be $\beta = 1.5$ in case of serviceability, according to DIN EN 1990. The load q and the prestressing loss P_{loss} are described as a priori, random variables, using Gaussian distributions with different mean values $\mu(q)\,\text{kN/m}$ and variance $\sigma(q) = 1\,\text{kN/m}$ for the load and a mean value $\mu(P_{\text{loss}}) = 10\,\%$ and variance $\sigma(P_{\text{loss}}) = 1\,\%$ for the prestressing loss. One optimization was performed for each of the various mean values of the load to investigate the influence of the load on the optimal amount of reinforcement. The fiber orientation parameter is considered as an interval $\lambda_f = [0.30; 0.45]$ for variant A and B. The total steel reinforcement is the sum of the support reinforcement $A_s = A_{s1} + A_{s2} + A_{s3}$ (see Figure 4 a) and Figure 5a)), where A_{s1} is kept constant as a minimum of $A_{s,min} = A_{s1} = 18\varnothing 16\,\text{mm}$ is needed according to the design guidelines, while A_{s2} and A_{s3} are within the interval $[4\,\varnothing\,8\,\text{mm}; 18\varnothing 16\,\text{mm}]$. This range was chosen since, considering the existing cross-section width of 2.85 m, it is not reasonable to place less than four rebars in one row and $18\varnothing 16\,\text{mm}$ per row is the existing amount of reinforcement of Variant A. For the optimization, the Particle Swarm Optimization (PSO) (Kennedy & Eberhart 1995) is applied with an extension to consider aleatory and epistemic uncertainties (Edler et al. 2019).

For the optimization, the FE simulations performed for each variant, is replaced by artificial neural networks (ANN) with feed forward architecture to speed up the computation time (Freitag et al. 2020). For all three variants, the same 150 models are generated, using Latin hypercube sampling (LHS) of prestress loss and amount of support reinforcement. In addition, for variant A and B the fiber orientation has been sampled as well. For variant A and B, an ANN with four input parameters (λ_f, P_{loss}, A_s and q), two layers with 10 and 5 hidden neurons and one output neuron w_{cr} (4-10-5-1) is sufficient to approximate the FE simulations with an accuracy of $R = 0.992$ for variant A and $R = 0.989$ for variant B, respectively. For variant B0, an ANN with three input parameters (P_{loss}, A_s and q), two layers with 8 and 4 hidden neurons and one output neuron w_{cr} (3-8-4-1) is adequate to approximate the FE simulations with an accuracy of $R = 0.908$. At this point, it should be noted that it is ensured that all ANN provide sufficiently accurate results especially in the range $w_{cr} \leq 0.2\,\text{mm}$, for subsequent optimization.

Figure 6 presents the results obtained by the ANN and the FE simulations for crack width versus fiber orientation and load for variant A (a) and B (b). It may be observed that the fiber orientation influences the crack width in variant B significantly more than for variant A, while the crack width increases for variant A at smaller load than for variant B independent of the fiber orientation.

3.3 *Results*

For a better illustration, the total amount of steel (sum of steel reinforcement and steel fibers) is presented in Figure 7 as the steel weight m rather than the area of steel A_s. In Figure 7a), the minimum required weight of steel reinforcement m_{rebar}, for which the constraint is fulfilled ($w_{cr}(A_s, q, \lambda_f, P_{loss}) \leq 0.2\,\text{mm}$), is given as a function of the mean value of the load, for variant A (black) and variant B (purple) for $\lambda_f = 0.30$ (dashed line) and 0.45 (solid line), for each variant and also for variant B0 (dotted line). The maximum load, at which the constraint is still fulfilled, is marked with a circle.

For variant A, the amount of reinforcement barely depends on the fiber orientation and much more one the mean value of the load. Only the minimum reinforcement is required, up to a mean value of the load of $\mu(q) = 93.2\,\text{kN/m}$ for $\lambda_f = 0.30$ and $\mu(q) = 93.5\,\text{kN/m}$ for $\lambda_f = 0.45$. With further increase in the load, the required amount of reinforcement increases, the maximum amount of reinforcement is required for $\lambda_f = 0.30$ at $\mu(q) = 98.0\,\text{kN/m}$ and for $\lambda_f = 0.45$ at $\mu(q) = 99.2\,\text{kN/m}$. At higher mean value of the load, the constraint ($w_{cr}(A_s, q, \lambda_f, P_{loss}) \leq 0.2\,\text{mm}$) is not fulfilled anymore. This means that, even with optimal fiber orientation, the serviceability limit state is not met at the design load of q = 100 kN/m, if uncertain loads and prestressing losses are taken into account.

For variant B, the minimum required amount of reinforcement is influenced by the fiber orientation and the mean value of the load. Only the minimum reinforcement is required, up to a load of $\mu(q) = 96.2\,\text{kN/m}$ for $\lambda_f = 0.30$ and $\mu(q) = 99.3\,\text{kN/m}$ for $\lambda_f = 0.45$. With further increasing mean value of the load, variant B requires rapidly more reinforcement for fiber orientation of $\lambda_f = 0.30$ as the the maximum amount of reinforcement is required at $\mu(q) = 99.4\,\text{kN/m}$, while for $\lambda_f = 0.45$ the maximum amount of reinforcement is not required until $\mu(q) = 103.5\,\text{kN/m}$. Consequently, the serviceability limit state is met for variant B, with consideration of uncertainties, for the design load as well as for higher mean value of the load but only for a good fiber orientation of $\lambda_f = 0.45$. Finally, comparing variant B and variant B0 (without fibers), it can be observed that, especially with a small amount of reinforcement, the fibers contribute significantly to the crack width reduction for any fiber orientation. If more reinforcement is required due to the load, the function of variant B rises just as quickly as one with fiber orientation $\lambda_f = 0.30$.

In Figure 7b), the minimum required total weight of steel ($m_{\text{tot}} = m_{\text{fibers}} + m_{\text{rebar}}$, where $m_{\text{fibers,A}} = 1.06\,\text{t}$, $m_{\text{fibers,B}} = 1.21\,\text{t}$ and $m_{\text{rebar}} = m_{\text{As,1}} + m_{\text{As,2}} + m_{\text{As,3}}$) is given as a function of the mean value of the load. Here, it can be seen that variant B is the most economical choice for a mean value of the load higher than $\mu(q) = 94\,\text{kN/m}$, if it can be ensured that $\lambda_f = 0.41$. Meaning, if a horizontal fiber orientation can be ensured, due to the casting process, and thus the interval range of the fiber orientation can be reduced to $\lambda_f = [0.410.45]$, variant B is to be preferred.

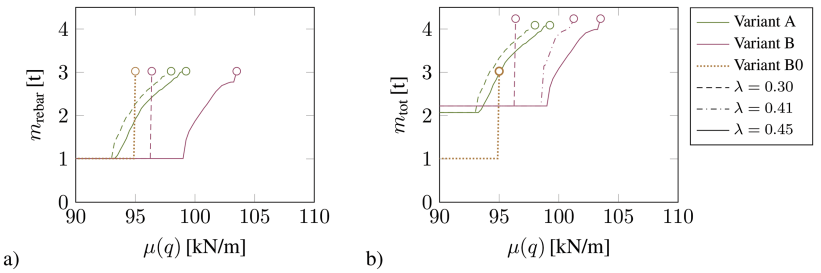

Figure 7. Optimization results for a) Weight of required reinforcement for different mean value of the load and b) Total weight of steel for different mean value of the load.

4 CONCLUSION

In this contribution, a prestressed bridge strengthened with fiber-reinforced concrete was investigated with respect to its maximum crack widths. It was observed that due to different types of concrete, cracks occur within the cross-section already at loads smaller than the design load. For this reason, an alternative cross-section of only two instead of there different concrete types has been presented (variant B). Variant B consists of a thicker fiber concrete layer with fewer but larger fibers, which significantly reduces the crack widths. In addition, less steel reinforcement is needed for the same load, and thus reducing the total amount of steel. In the next step, in addition to the cracks above the support, the cracks in the field should also be investigated, as well as the load-bearing capacity of both variants. Moreover, it would also be possible to add the concrete layer thickness as additional design variable in order to also optimize the required concrete material volume.

ACKNOWLEDGMENT

The authors gratefully acknowledge the financial support of the German Research Foundation (DFG) within Subproject 6 (Project number 312921814) of the Priority Programme "Polymorphic uncertainty modelling for the numerical design of structures - SPP 1886".

REFERENCES

Edler, P., S. Freitag, K. Kremer, & G. Meschke (2019). Optimization approaches for the numerical design of structures under consideration of polymorphic uncertain data. *ASCEASME Journal of Risk and Uncertainty in Engineering Systems Part* B: *Mechanical* Engineering *5*(4), 041013 (12 pages).

European Comittee for Standardisation (2005). *EN 1992 - Eurocode 2: Design of concrete structures. European Committee for Standardisation*

Freitag, S., P. Edler, K. Kremer, & G. Meschke (2020). Multilevel surrogate modeling approach for optimization problems with polymorphic uncertain parameters. *International Journal of Approximate Reasoning 119*, 81–91. Special issue on Computing with confidence.

Gall, V. E., S. Butt, G. Neu, & G. Meschke (2018). An embedded rebar model for computational analysis of reinforced concrete structures with applications to longitudinal joints in precast tunnel lining segments. In G. Meschke, B. Pichler, and J. G. Rots (Eds.), *Computational Modelling of Concrete Structures (EURO-C 2018)*, pp. 705–714. CRC press.

Gudzulic, V. & G. Meschke (2021). Multi-level approach for modelling the post-cracking response of steel fibre reinforced concrete under monotonic and cyclic loading. *Proceedings in Applied Mathematics and Mechanics.*

Gudzulic, V., G. Neu, G. Gebuhr, S. Anders, & G. Meschke (2020). Numerisches Mehrebenen-Modell für Stahlfaserbeton: Von der Faser- zur Strukturebene. *Beton und Stahlbetonbau 115*, 146–157.

Holschemacher, K., F. Dehn, T. Müller, & F. Lobisch (2017). *Betonkalender 2017*, Chapter Faserbeton. Ernst und Sohn.

Kennedy, J. & R. C. Eberhart (1995, November-December). Particle swarm optimization. In *Proceedings of the IEEE International Conference on Neural Networks*, Piscataway, NJ, USA, pp. 1942–1948. IEEE Press.

Möller, B. & M. Beer (2008). Engineering computation under uncertainty – Capabilities of non-traditional models. *Computers and Structures 86*, 1024–1041.

Ortiz, M. & A. Pandolfi (1999). Finite-deformation irreversible cohesive elements for threedimensional crack-propagation analysis. *International Journal for Numerical Methods in Engineering 44*(9), 1267–1282.

Pelke, E., A. Jaborek, D. Berger, & E. Brühwiler (2018). Überführungsbauwerk der L3378 bei Fulda-Lehnerz – Erster Einsatz von UHFB in Deutschland im Straßenbrückenbau, Teil 1: Projektentwicklung und Baudurchführung. *Beton- und Stahlbetonbau 113*(11), 831–841.

Tiberti, G., F. Germano, A. Mudadu, & G. Plizzari (2018). An overview of the flexural postcracking behavior of steel fiber reinforced concrete. *Structural Concrete 19*, 695–718.

Wang, Y., S. Backer, & V. Li (1989). A statistical tensile model of fibre reinforced cementitious composites. *Composites 20(3)*, 265–274.

Zhan, Y. & G. Meschke (2016). Multilevel computational model for failure analysis of steelfiber - reinforced concrete structures. *Journal of Engineering Mechanics (ASCE) 142* (11), 04016090 (1–14).